Computational Models of Functional Hyperaemia in the Cerebro-vasculature

T. David[1], S. Alzaidi[1], H. Farr[1]

[1]Centre for Bioengineering, University of Canterbury, New Zealand
Email:tim.david@canterbury.ac.nz

Abstract: The combination of an autoregulation model with a fully populated arterial tree able to regulate dynamically remains a relatively unexplored field. A non-dimensional representation of autoregulation coupled with an asymmetric binary tree algorithm (approx 1,000,000 vessel segments) simulating the cerebro-vasculature has been developed. Results are presented for an autoregulation algorithm of the cerebro-vasculature downstream of the efferent arteries, in this case the middle cerebral artery. In addition the model is capable of simulating spatially local variation in the metabolic rate and thus enabling local dilations of the vasculature. This is termed functional hyperaemia and is the phenomenon associated with the brain's ability to provide variations in nutrients to specific sites within the brain cortex when the person is processing certain tasks. A new metabolic model for autoregulation has been developed and this allows carbon dioxide to diffuse between arterioles and the venous bed causing either a relaxation of contraction of the nearby arteriolar bed. Results show that under variations in pressure the metabolic mechanism provides sufficient variation in the peripheral resistance to accommodate constancy of cerebral blood perfusion. Secondly the spatial distribution of vessel radii is altered under functional hyperaemia and results provide a relationship between increases/decreases in metabolic rate and the vessel radial distribution of the cerebrovasculature, thus indicating that the metabolic process is the essential driving agent for cerebral processing. The authors believe this to be the first time a full arterial tree algorithm for the cerebrovasculature has been developed to show both the autoregulation and functional hyperaemia mechanisms.

1   INTRODUCTION

Cerebral tissue requires a constancy of both oxygen and nutrients (notably glucose). During periods of pressure variation, which occur throughout the normal day as well as in cases of pathological hypo- and hyper-tension, the body's cerebral autoregulation mechanism cause the arterioles to vasoconstrict/dilate in response to changes in cerebral perfusion pressure over a certain range, thus maintaining a relatively constant cerebral blood flow. These effects are of particular importance when investigating how blood is redistributed not only via the circle of Willis but throughout the cerebral tissue. It should be noted that there have been a number of cerebral autoregulation models proposed [1] [2], [3], including models incorporated with a circle of Willis [4], [5], [6], [7], [8], [9] [10]. However, the combination of an autoregulation model with a fully populated arterial tree able to regulate dynamically remains a relatively unexplored field. Particular interest has focused on the myogenic mechanism where the systemic blood pressure exerts an influence on vascular smooth muscle, an excellent review can be found in [11]. Fundamental studies were carried out by Harder [12, 13]and Harder et al [14]. Less research has been done for the metabolic condition where variations in pH and CO_2 are considered to be the prime movers for dilation/contraction of the small arterioles deep in the vascular tree. The most comprehensive study of blood flow control has been that of [15], however even in this case several important constants remain unknown making the model somewhat constrained. We have shown [16] that the myogenic model mediates vessel contraction only at relatively high pressures (essentially proximal to the major cerebral vessels areas) rather than at the arteriolar level. In addition the majority of peripheral resistance occurs at the distal end of the vascular bed where the vessel diameters are of the order of $100 \mu m$. In this particular model we therefore neglect the myogenic response to pressure variations and concentrate solely on the metabolic simulation. The present model in determining the vascular tree uses previous work by [17]. In order to allow all parts of the tree to vary in its arterial radius (and hence resistance) the metabolic model is non-dimensionalised enabling a single algorithm to be utilised.

2 THEORY AND METHODOLOGY

The models for both myogenic and metabolic autoregulation were constructed with the aim of simplicity in formulation as much as possible while still upholding the correct experimentally observed observations. The myogenic model is based on the original work of Gonzalez-Ferrandez and Ermentrout [18] here termed the GFE model. Complete details of the original GFE model its assumptions and how it was implemented into a vascular tree can be found in [18] and [16] resp.

2.1 Metabolic Model

Although selective ion channels in the smooth muscle cell of the cerebro-vasculature respond to variations in both CO_2 and pH our initial model for the metabolic response uses the simple assumption that the set of arterioles feeding the capillary bed are in close proximity to the venous return. Excess carbon dioxide in the venules is diffused to the arterioles and induces a relaxation/contraction of the arteriolar radius thus allowing increased/decreased blood flow to convect away carbon dioxide and hence maintain the correct CO_2 concentration. This model was also used in the 1D models of [19]. Equation (2.1) represents a conservation equation where the rate of change of carbon dioxide is balanced by the production (due to metabolism) and that convected away by the blood flow.

$$\frac{d}{dt}CO_{2,tissue} = CMRO_2 + CBF\left(CO_{2,artery} - CO_{2,tissue}\right)$$

(0.1)

where $CO_{2,tissue}$ is the tissue concentration of carbon dioxide, $CO_{2,artery}$ is the arterial concentration of carbon dioxide (assumed to be 0.49ml/ml) $CMRO_2$ is the cerebral metabolic rate of oxygen consumption (assumed to be a constant 0.035ml/g/min for all parts of the brain), which due to the stoichiometry of the aerobic metabolism in the brain tissue, is equal to the cerebral metabolic rate of carbon dioxide production. CBF is the flow rate in the terminal artery and thus entering the capillary bed. We use a reverting differential equation for the radius of the arteriole given by

$$\frac{dr}{dt} = \frac{1}{\tau}\left(CO_{2,sp} - CO_{2,tissue}\right)$$

(0.2)

here $CO_{2,sp}$ is the steady state ($\frac{d}{dt}\left(CO_{2,tissue}\right) = 0$) solution to (2.1) using CBF_0 and τ is a characteristic time for the arterial smooth muscle cells to react. We choose the following non-dimensionalisation

$$c = \frac{CO_{2,tissue}}{CO_{2,artery}}; \ t = \frac{T}{CBF_0}; \ \xi = \frac{r}{r_0}$$

(0.3)

where r_0 is the arterial radius and CBF_0 is the value of the blood flow in the terminating arteriole at normal physiological conditions (known quantities). CBF is evaluated by recalculating the vascular resistance of the tree as outlined in section 3.1 below. With the above equations (2.1 and 2.2) become

$$\frac{dc}{dT} = \left(\psi - 1\right) + Q\left(1 - c\right); \frac{d\xi}{dT} = -\zeta\left(\psi - c\right)$$

(0.4)

With

$$Q = \frac{CBF}{CBF_0}; \ \psi = 1 + \frac{CMRO_2}{CO_{2,artery}CBF_0}; \ \zeta = \frac{CO_{2,artery}}{\tau r_0 CBF_0}$$

2.2 Asymmetric binary tree model

The tree branching algorithm used is that developed for the abdominal fractal vascular network of Olufsen et al [17] and is based on two variables: a power exponent k (describing the relationship between parent vessel
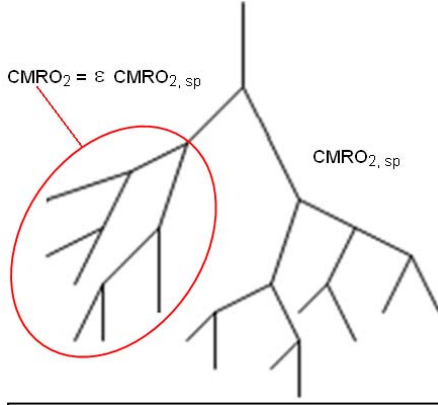
David *et al.*, Computational Models of Functional Hyperaemia in the Cerebro-vasculature

Figure 1: A local area of the tree with variation in the metabolic rate

.

radius r_p and daughter vessels radii r_{d1} and r_{d2}, and an asymmetry ratio γ (describing the relative ratio between two daughter vessels). For this particular study a binary tree emulates the vascular system stemming from a major artery, say the middle cerebral artery (MCA) for example. The values of k and γ change depending on the location of the vessel in the tree-i.e. values are different for arteries, arterioles and capillaries. The length and radius of a vessel are related by a length to radius ratio (denoted l_{rr} and chosen as 20 for this model). Here we take values of k and γ as those given in [17]. Figure 1 shows a sketch of the basic network indicating an area of variable metabolic rate.
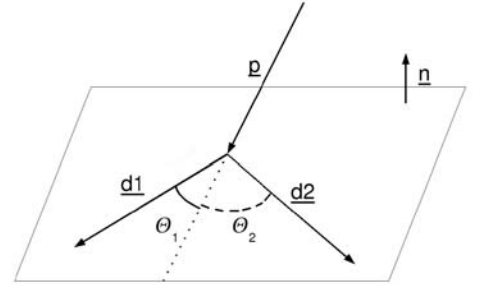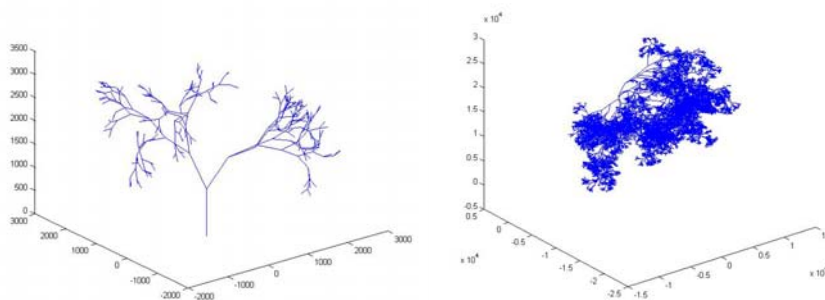
The model has the ability to emulate actual vascular networks by using the statistical data of Lauwers et al [20] (data of radii and length of all vessels in a small section of the cortex). The mean and the standard deviation from this data population is implemented into the code so that each arterial segment in the tree has a probability density function that emulates this physiological data. Additionally we are able to define trees in 3D by finding the coordinates of a daughter vessel when it is born. With volume minimizing considerations, Kamiya and Togawa [21] showed in their studies that the angles $\theta_{1,2}$ (see Figure 2) between a parent and its daughters are a function of their radius as shown in equation (2.5).

Figure 2: daughter artery angles and their corresponding plane.

$$\cos\theta_1 = \frac{r_p^4 + r_{d1}^4 - r_{d2}^4}{2r_p^2 r_{d1}^2}$$

$$\cos\theta_2 = \frac{r_p^4 + r_{d2}^4 - r_{d1}^4}{2r_p^2 r_{d2}^2}$$

(0.5)

For each daughter, there are three unknowns (the coordinates of the upper extremity) so three equations are needed. By fixing the length and this angle there are two equations. The last equation says that the two daughters belong to the same plane (n is the normal of this plane) and the coordinates of n are drawn randomly with a uniform density. This randomization allows for "forcing" the arteries to grow in particular directions as used by Schreiner et al [22]. Hence we can write the following constraints

$$\langle d,n\rangle = 0$$
$$\|\mathbf{d}\|_2 = L$$
$$\langle \mathbf{p},\mathbf{d}\rangle = \cos\theta \|\mathbf{d}\|_2 \|\mathbf{p}\|_2$$

(0.6)

Unfortunately, this system is non-linear and hence solved with an iterative method. The Newton-Raphson method has been chosen in this case.

Now $\mathbf{F}(\mathbf{d}) = 0$ is solved using a Newton-Raphson algorithm where $\mathbf{F} : \Box^3 \rightarrow \Box^3$ is defined by

$$\mathbf{F}(\mathbf{d}) = \begin{pmatrix} xn_x + yn_y + zn_z \\ x^2 + y^2 + z^2 - L^2 \\ xp_x + yp_y + zp_z - \cos\theta L\|\mathbf{p}\|_2 \end{pmatrix} ; \mathbf{d} = \begin{pmatrix} x \\ y \\ z \end{pmatrix}, \mathbf{p} = \begin{pmatrix} p_x \\ p_y \\ p_z \end{pmatrix} \text{ and } \mathbf{n} = \begin{pmatrix} n_x \\ n_y \\ n_z \end{pmatrix}$$

(0.7)

Figure 3a) 313 segments (root = 50 μm)   3b) 13,987 segments (root = 200 μm)

Figures 3a) and 3b) show examples of trees grown in 3D with varying sizes of root vessel (the terminating vessel size was always 10 μm)

2.3   Peripheral Resistance and pressure Distribution Evaluation

To find each individual resistance of each segment in the tree the algorithm uses a Poiseuille flow assumption such that the resistance of an arterial segment is proportional to the inverse of the fourth power of the radius. The viscosity is calculated using the diameter dependent equations from Pries and Secomb [23]. In order to find the flow and pressure distribution throughout the tree a single pass up and down the tree is required. Starting at each terminal segment a total resistance is evaluated for the two daughters and the parent artery assuming that the terminal segments are connected via the venous bed (essentially daughters in parallel with the parent in series). This parallel/series calculation is then done at each bifurcation of the tree until there is a single value of resistance. The total flow into the arterial tree is known and hence the total pressure drop can be evaluated. Moving down the tree the pressure drop and flow rate at and through each arterial segment is calculated respectively.

The trees used to produce the results in this paper consist of approximately 1,000,000 segments of which 500,000 are terminal segments. The blood pressure at the inlet to the MCA (Pa) and the venous pressure (Pv) at the end of the tree are both inputs.

2.4   Capillary Bed

At each terminal segment the capillary bed consists of approximately 6,000 capillaries in parallel, each of which is modelled as an identical Krogh cylinder, and as analysed by Bloch [24] and Blum [25]. The number of capillaries is determined by the known perfused volume of brain tissue for that particular major efferent artery. Although both Bloch and Blum provided analytical solutions (for the steady-state condition) of oxygen consumption in a capillary the algorithm used in this simulation for evaluating the oxygen and carbon dioxide concentration within the cylinder is that given by McGuire and Secomb [26] details of which need not be given here.

3   NUMERICAL METHODS

The differential equations, (2.4) were solved using MATLAB's ode23s routine (based on a modified Rosenbrock formula of order 2. Despite the fact that transmural pressure and wall shear stress are coupled, they are treated as being independent for the purpose of simplicity of solution. Therefore, to calculate the response of an artery to wall shear stress and pressure, the pressure increment method described above is used assuming that wall shear stress is kept constant at each pressure step.

Values of the non-dimensional radius once they have reached an asymptotic value are stored in a data set of radius, wall shear stress and pressure creating a "look-up table". In order to change each arterial radius in the entire tree a bilinear interpolation method is used such that with a given wall shear stress and pressure the new radius of each artery is found in conjunction with the cerebral arterial tree model.

3.1   Solution of autoregulation model with the Asymmetric binary tree

All initial flow rates, pressure drops, and radii of all tree segments are calculated at the creation of the arterial tree as described above and using a known value of the initial radius (in this case the middle cerebral artery

(1mm) and a systemic pressure of 75 mmHg. This pressure value is derived from the 3D computational model of [4] to take into account the pressure drop through the circle of Willis. The WSS value and the pressure are used with the "look-up table" to find the corresponding radius value for each segment. All pressures and flowrates are then recalculated throughout the arterial tree with these new radii values by traversing up and down the tree to evaluate new pressures and flow rates. This process is then repeated until a simple convergence criterion on the total peripheral resistance is met. For each pressure value ranging from zero to 200 mmHg and for each pressure value in the tree the radii of segments, where these radii lie between 10 and 100 μm, are changed in an iterative manner (using the look-up table previously evaluated from equations (2.4) until a converged value of the total peripheral resistance is found. Segments of the tree with radii outside of the range given above are unchanged.
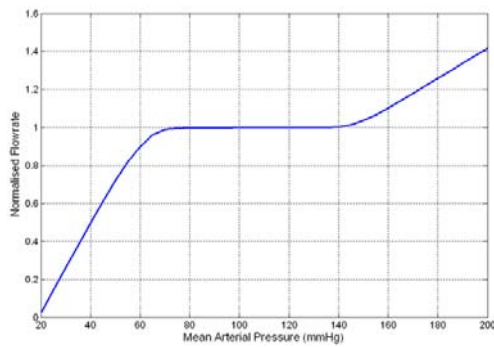
4   RESULTS

4.1   Autoregulation model

Figure 4a) plots physiological perfusion pressure vs the total normalised flow rate in the tree. This flow rate is normalised to that known value $2.85\ mL\ s^{-1}$ required to perfuse the volume of the brain supported by the middle cerebral artery at "normal" physiological conditions (systemic pressure of 100 mmHg). Both equations for the tissue concentration of carbon dioxide and the arterial radius provide stable equilibria. If the carbon dioxide increases the sign of the rate of change changes (similarly for the radius) and thus always reverting t the steady state. Linearisation of these equations shows the eigen values to real and negative.
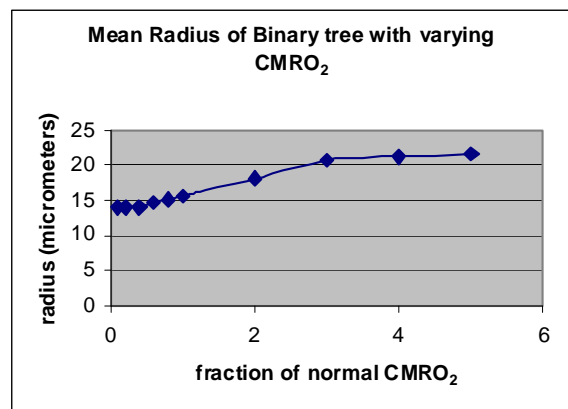

Figure 4 a) Normalised autoregulation curve

4.1.1   Metabolic

It has been experimentally shown by Lipowsky et al [27] that the large collection of small arterioles makes up the majority of the resistance of an arterial tree. It has been shown [16] that the current myogenic autoregulation model does not provide enough radial change in these smaller arterioles to facilitate the ideal autoregulation profile.

As shown in Figure 1 we choose a small portion of cerebral tissue by choosing a branch of the vascular tree and increase/decrease the metabolic rate above/below that given by $CMRO_2 = 0.035$ by a factor ε. Figure 4b shows the variation in mean radius of the vessels in the specified branch as a function of ε. As ε increases then the radius also increases to allow more blood and nutrients to flow to the **local**

Figure 4 b) mean radius vs metabolic trate

area of tissue. It is noted that the rest of the tree varies but at an insignificant level. Figures 5a) and 5 b) show the change in distribution of the radius for values of $\varepsilon = 1$ and 1.5 after a drop in perfusion pressure of 20 mmHg. This drop in pressure induces the autoregulation mechanism to act. It is seen from Figures 5 a) and b) that even though the model does not include "upstream" effects and although the smaller vessels change the most the larger arterioles due have a substantial effect thus providing a reduction in the peripheral resistance of the tree.

It is also interesting to note the bifurcation angles $\theta_{1,2}$ that occur in the tree for various values of k and γ.

Table I shows the values of γ and k used in the three sections of the tree defined by the range of radii and their respective angles , including the total angle of bifurcation. In contrast to anatomical measurements the angles calculated here are higher than expected. However it has been shown by Avolio and others [28] that this does not necessarily affect the peripheral resistance significantly nor the dynamics (impedance).

Table I

Radius range (μm)	$250 \le r$	$50 \le r \le 250$	$r \le 50$
γ	0.4	0.6	0.9
k	2.5	2.76	2.9
θ_1 (degrees)	51.87865	59.50674	69.36147
θ_2 (degrees)	59.65198	48.25407	23.00454
$\theta_1 + \theta_2$ (degrees)	111.5306	107.7608	92.36601
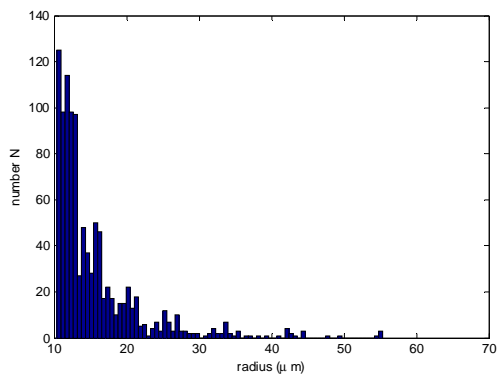
Figure 5a) distribution of radii for 1*CMRO$_2$, ,   Figure 5b) distribution of radii for 1.5*CMRO$_2$
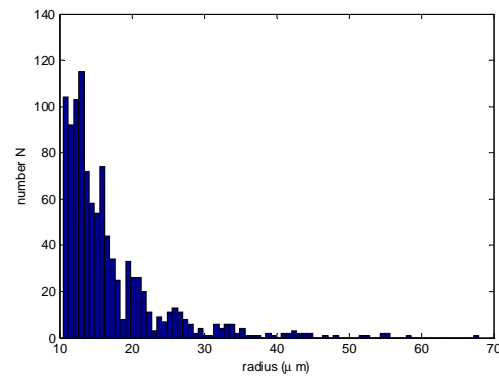
5   DISCUSSION AND CONCLUSIONS

By developing a non-dimensional representation of the arterial wall model and the asymmetric binary tree algorithm of Olufsen et al [17] results are presented for an autoregulation algorithm of the cerebro-vasculature downstream of the efferent arteries, in this case the middle cerebral artery.

A relatively simple metabolic model has been developed under the assumption of close proximity between venules and the vascular tree at the arteriolar level (this close proximity is certainly true in the case of fish!). The model allows carbon dioxide to diffuse between arterioles and the venous bed causing either a relaxation or contraction of the nearby arteriolar bed. By comparing with a myogenic mechanism [16] (results not shown) it indicates that the metabolic mechanism seems to be the dominant mechanism for cerebral autoregulation due to the majority of vascular resistance occuring at the arteriolar level. In addition by specifying areas of varying metabolic rate the model can simulate the local autoregulation process.

The authors believe this to be the first time a full arterial tree algorithm has been developed to show the autoregulation mechanism and especially that of local perfusion variations simulating functional hyperaemia. However it is thought that the time taken for carbon dioxide to diffuse into the tissue [29] is longer than the characteristic timescales measured for blood vessels to alter their radii in response to local brain activity. Further developments by the group here at Canterbury in this particular area of modeling the autoregulation mechanism in the brain are aimed at integrating a more complex metabolic model into the vascular tree framework. This metabolic model includes a number of cellular processes which affect the calcium inside both the smooth muscle cell and the endothelial cell. From a mathematical perspective this involves the inclusion of a significant number of ordinary differential equations, particularly in modeling the calcium concentration in an associated glial cell called an "astrocyte" and the inwardly rectifying potassium channels which present themselves on the membrane of the smooth muscle cell. The astrocyte can be considered as the "bridge" from synapse to the local blood supplying vessel [30]. One end of the glial cell is located in close proximity to the post-synaptic neuron whilst the other end is firmly fixed around the vessel wall. It is thought that calcium variations cause potassium channels to open and provide "surges" of potassium into the extra-cellular space. The particular potassium channels on the blood vessel in response to these "surges" tend to

hyperpolarise the smooth muscle cell thereby dilating the vessel and allow more blood to flow to the brain tissue and experimental evidence tends to suggest that this is crucial in the local support of neuronal activity [31, 32]. We are therefore now able to model different cellular mechanisms in different parts of the vasculature, particularly utilising the myogenic model for the larger arteries and the more complex "astrocyte" model at the deeper levels of the vascular tree. This requires considerable compute power and as such we will utilise this model in conjunction with distributed memory computer architectures such as the IBM Blue Gene (http://www.bluefern.canterbury.ac.nz/): mapping each part of the vasculature on to each Blue Gene node and allowing the subset of o.d.e.s which represent different cellular processes to simulate the full tree as a whole "organ".

ACKNOWLEDGMENTS

REFERENCES

1. Ursino, M. and M. Giulioni, *Quantitative assessment of cerebral autoregulation from transcranial Doppler pulsatility: a computer simulation study.* Medical Engineering and Physics, 2003. **25**(8): p. 655-666.
2. Ursino, M., *A mathematical model of overall cerebral blood flow regulation in the rat.* IEEE Trans Biomed Eng, 1991. **38**(8): p. 795-807.
3. Olufsen, M.S., A. Nadim, and L.A. Lipsitz, *Dynamics of cerebral blood flow regulation explained using a lumped parameter model.* Am J Physiol Regul Integr Comp Physiol, 2002. **282**(2): p. R611-622.
4. Moore, S.M., et al., *3D Models of Blood Flow in the Cerebral Vasculature.* Journal of Biomechanics, 2006. **39**(8): p. 1454-1463.
5. Moore, S. and T. David, *Auto-regulated Blood Flow in the Cerebral-Vasculature.* Journal of Biomechanical Science and Engineering (JSME), 2006. **1**(1): p. 1-14.
6. Moore, S.M., et al., *One-Dimensional and Three-Dimensional models of Cerebrovascular Flow.* Journal of Biomechanical Engineering, 2005. **127**: p. 440-449.
7. Moorhead, K.T., et al., *Lumped Parameter and Feedback Control Models of the Auto-regulatory Response in the Circle of Willis.* Computer Methods in Biomechanics and Biomedical Engineering, 2004. **7**(3): p. 121-130.
8. Moorhead, K.T., et al., *Metabolic Model for Autoregulation in the Circle of Willis.* Journal of Biomechanical Engineering, 2006. **128**(3): p. 462-466.
9. Moorhead, K.T., et al., *Impact of Decentralised control in cerebral blood flow auto-regulation using 1D and 3D models.* International Journal of Intelligent Systems, Technologies and Applications, 2005. **1**(1/2): p. 95-110.
10. David, T., M. Brown, and A. Ferrandez, *Auto-Regulation and Blood Flow in the Cerebral CIrculation.* Int. Jour. Num. Methods Fluids, 2003. **43**: p. 701-713.
11. Haga, J.H., Y.S. Li, and S. Chien, *Molecular basis of the effects of mechanical stretch on vascular smooth muscle cells.* J Biomech, 2007. **40**(5): p. 947-60.
12. Harder, D.R., *Pressure-dependent membrane polarisation in cat middle cerebral artery.* Circulation Research, 1984. **55**: p. 197-202.
13. Harder, D.R., *Pressure-induced myogenic activation of cat cerebral arteries is dependent on intact endothelium.* Circ Res, 1987. **60**(1): p. 102-7.
14. Harder, D.R., R.J. Roman, and D. Gebremedhin, *Molecular mechanisms controlling nutritive blood flow: role of cytochrome P450 enzymes.* Acta Physiol Scand, 2000. **168**(4): p. 543-9.
15. Banaji, M., et al., *A physiological model of cerebral blood flow control.* Mathematical Biosciences, 2005. **194**(2): p. 125-173.
16. David, T., H. Farr, and S. Alzaidi, *Coupled Autoregulation Models in the Cerebro-vasculature".* Journal of Engineering Mathematics, 2009 **DOI: 10.1007/s10665-009-9274-2**.
17. Olufsen, M.S., M.S. Steele, and C.A. Taylor, *Fractal Network model for simulating abdominal and lower extremity blood flow during reesting and exercise conditions.* Computer Methods in Biomechanics and Biomedical Engineering, 2007. **10**: p. 39-51.
18. Gonzalez-Ferrandez, J.M. and B. Ermentrout, *On the origin and dynamics of the vasomotion of small arteries.* Mathematical Biosciences, 1994. **119**: p. 127-167.
19. Alastruey, J., et al., *Reduced modelling of blood flow in the cerebral circulation: Coupling 1-D, 0-D and cerebral auto-regulation models.* Int. Jour. Num. Methods Fluids, 2008. **56**: p. 1061-1067.

20. Lauwers, F., et al., *Morphometry of the human cerebral cortex microcirculation: General characteristics and space-related profiles.* NeuroImage, 2008. **39**: p. 936-948.

21. Kamiya, A. and T. Togawa, *Optimal Branching Structure of the Vascular Tree.* Bulletin of Mathematical Biophysics, 1972. **34**: p. 431-438.

22. Schreiner, W. and P.F. Buxbaum, *Computer-Optimization of Vascular Trees.* IEEE Trans Biomed Eng, 1993. **40**(5): p. 482-491.

23. Pries, A.R. and T.W. Secomb, *Microvascular blood viscosity in vivo and the endothelial surface layer.* Am Heart J - Heart Cir. Phys., 2005. **289**: p. H2657-H2664.

24. Bloch, I., *Some Theoretical considerations concerning the interchange of metabolite between capillaries and tissue.* Bulletin of Mathematical Biophysics, 1943. **5**: p. 1-14.

25. Blum, J.J., *Concentration profiles in and around capillaries.* American Journal of Physiology, 1960. **198**(5): p. 991-998.

26. McGuire, B.J. and T.W. Secomb, *A theoretical model for oxygen transport in skeletal muscle under conditions of high oxygen demand.* J Appl Physiol, 2001. **91**(5): p. 2255-65.

27. Lipowsky, H.H.K. and B.W. Zweifach, *The distribution of blood rheological parameters in the microvasculature of the cat mesentary.* Circulation Res 1978. **43**: p. 738-749.

28. Beard, D.A. and J.B. Bassingthwaighte, *The Fractal nature of Myocardial Blood FLow Emerges from a Whole-Organ Model of Arterial Network.* Journal of Vascular Research, 2000. **37**(4): p. 282-296.

29. Vaughn, M.W., L. Kuo, and J.C. Liao, *Effective diffusion distance of nitric oxide in the microcirculation.* Am J Physiol, 1998. **274**(5 Pt 2): p. H1705-14.

30. Takano, T., et al., *Astrocyte-mediated control of cerebral flow.* Nature Neuroscience, 2006. **9**(2): p. 260-267.

31. Filosa, J. and V.M. Blanco, *Neurovascular coupling in the mammalian brain.* Experimental Physiology, 2007. **92**: p. 641-646.

32. Filosa, J., et al., *Local Potassium signalling couples neuronal activity to vasodilation in the brain.* Nature Neuroscience, 2006. **9**(11): p. 1397-1403.